2014

A Method to Represent Heterogeneous Materials for Rapid Prototyping: The Matryoshka Approach

Shuangyan Lei
Iowa State University

Matthew C. Frank
Iowa State University, mfrank@iastate.edu

Donald D. Anderson
University of Iowa

Thomas D. Brown
University of Iowa

HHS Public Access

Author manuscript

Rapid Prototyp J. Author manuscript; available in PMC 2015 June 25.

Published in final edited form as:

Rapid Prototyp J. 2014 ; 20(5): 390–402. doi:10.1108/RPJ-10-2012-0095.

A Method to Represent Heterogeneous Materials for Rapid Prototyping: The Matryoshka Approach

Shuangyan Lei[*], **Matthew C. Frank**[*], **Donald D. Anderson**[†], and **Thomas D. Brown**[†]

[*]Department of Industrial and Manufacturing Systems Engineering; Iowa State University, Ames, Iowa, USA

[†]Department of Orthopaedics and Rehabilitation; The University of Iowa, Iowa City, Iowa, USA

Abstract

Purpose—The purpose of this paper is to present a new method for representing heterogeneous materials using nested STL shells, based, in particular, on the density distributions of human bones.

Design/methodology/approach—Nested STL shells, called Matryoshka models, are described, based on their namesake Russian nesting dolls. In this approach, polygonal models, such as STL shells, are "stacked" inside one another to represent different material regions. The Matryoshka model addresses the challenge of representing different densities and different types of bone when reverse engineering from medical images. The Matryoshka model is generated via an iterative process of thresholding the Hounsfield Unit (HU) data using computed tomography (CT), thereby delineating regions of progressively increasing bone density. These nested shells can represent regions starting with the medullary (bone marrow) canal, up through and including the outer surface of the bone.

Findings—The Matryoshka approach introduced can be used to generate accurate models of heterogeneous materials in an automated fashion, avoiding the challenge of hand-creating an assembly model for input to multi-material additive or subtractive manufacturing.

Originality/Value—This paper presents a new method for describing heterogeneous materials: in this case, the density distribution in a human bone. The authors show how the Matryoshka model can be used to plan harvesting locations for creating custom rapid allograft bone implants from donor bone. An implementation of a proposed harvesting method is demonstrated, followed by a case study using subtractive rapid prototyping to harvest a bone implant from a human tibia surrogate.

Keywords

Rapid prototyping; Rapid manufacturing; Heterogeneous object modeling; Bone implant

1. Background

Among the extraordinary capabilities of current Additive Manufacturing (AM) is the recent ability to create parts with varying material properties. Some example AM techniques include Three Dimensional Printing (3DP), Laser Engineered Net Shaping (LENS), and Polyjet Technologies, which can make parts with multiple materials, or at least designate

multiple components in color (3DP). In particular, the multi-material 3D printing system Connex500™developed by Objet Ltd. has the capability of printing parts made of up to fourteen different materials in a single print. Multi-material or *heterogeneous* materials, in general, involve objects with spatially different material compositions or structures [1,2]. Recently, heterogeneous components have attracted research interest, and extensive work has been undertaken in the area of heterogeneous object modeling in CAD.

Simultaneously, there has also been considerable research in the biomedical and Rapid Prototyping (RP) communities to address the challenge of creating custom bone implants. Biomedical implant manufacturing using AM has made significant progress in fabricating patient-specific implants. These techniques include Selective Laser Melting (SLM), Stereolithography (SLA), Electron Beam Melting (EBM), Direct Metal Laser Sintering (DMLS), 3DP, LENS, etc. SLM has been shown to be a useful process to manufacture 3D porous metallic structures using a variety of material options, including stainless steel, titanium, and chromium-cobalt [3]. EBM technology has been relatively widely used to fabricate custom-designed implants for knees, hips, elbows, shoulders, fingers, and bone plates in titanium alloy (Ti6A14V) [4,5]. LENS has also been developed to make load-bearing metal porous implants with complex anatomical shapes from materials like Ti, Ti6A14V, Ni-Ti and CoCrMo alloys. The surface porosities and load-bearing properties of such manufactured implants depend on parameters like laser power, power feed rate, and scan speed [6–8]. SLA can be used to create tissue geometry of arbitrary 3D shapes directly from CAD data, and low-density cellular materials with gaseous voids can be manufactured by SLA technologies [9]. This cellular structure material facilitates bone ingrowth for biological fixation, such as the case with acetabular implants designed with preferential porosity gradients for use in hip replacement [10].

Existing CAD models investigating this topic fall into two categories, which are *evaluated* models and *unevaluated* models, depending on the representational exactness and compactness [11]. Evaluated models are inexact, and represent heterogeneous material distributions through intensity-space decompositions. Typical examples are the voxel models [12,13] and volume mesh based models [14]. Unevaluated models utilize exact geometric data representation and rigorous functions to represent the material distributions. Examples include explicit functional representations [15–17], control feature-based models [18–21], control point-based models [22], and implicit function-based models [23].

A variety of heterogeneous object modeling methods have been presented in the literature; however, challenges remain with representation of the complex models that RP systems can manufacture. This is true not only for multi-materials, but for other complex geometries in general. For example, additive RP machines can create complex scaffolds, but new methods are still under development for easy and computationally efficient representation of models such as bone scaffolds, biomimetic objects, etc.

One particularly challenging heterogeneous material is bone. Clinically, at present, there is very strong preference for usage of native bone to reconstruct defects commonly resulting from severe trauma, from excision of bone tumors, and from biologically mediated loss of bone around failed or failing joint replacements. The patient’s own bone (an autograft) is

most preferred for such purpose, but options for sites from which to harvest autograft obviously are very limited. Bone from a deceased donor (allografts) is by far the most commonly used alternative. Surgeons often are faced with the problem of shaping part of an allograft donor bone to fit an irregularly-shaped defect in a living patient's bone, configuring the allograft so as to approximately match the patients' original density distribution.

Native human bone's density distribution from inside to outside spans a significant range. To illustrate, Figure 1 shows a cross-sectional view of a femur bone, showing the spongy, low density trabecular bone in the middle, versus the high-density cortical bone on the outside. There have been numerous research efforts to model the density of bone. For example, Yao and Taylor [24] used a Bernstein polynomial in barycentric coordinates to model density variations. Bibb and Sisias [25] used SLA techniques to build cancellous bone structure models, and investigated the problems associated with the CAD models saved in STK and SLC file formats, respectively. Chen *et al*. [26] put forward a technique to fabricate the mold of an artificial bone, composed of a nontoxic soluble material, by using two CAD models: an external contour CAD model, and an internal microtubule structure CAD model. The external contour model is obtained by reconstructing the 3D geometry from bone CT scan data and saved to STL format. The internal microtubule structure model was built up through micrographs and histological analysis. Fang *et al.* [27] proposed a multi-scale voxel modeling approach to model the bone structure at macroscopic and microscopic levels, and developed a Direct Fabrication (DF) system to fabricate a tissue scaffold constructed with a random heterogeneous microstructure and designed shape. Sun *et al.* [28] presented a method to develop a femur model by using quantitative CT numbers (QCTN) to characterize the bone mechanical properties. It used different QCTN to characterize the density of the tissue in different layers and considered both cancellous and cortical bone smeared together as one structure in each layer.

Currently, there is no effective modeling approach to characterize the heterogeneity of bone structure, let alone any method that would enable automated process planning in a rapid prototyping system. This paper focuses on the challenge of representing multi-material bone properties from CT scan data, a widely used medical imaging modality that represents x-ray attenuation properties (which scale with density) as grayscale image intensity distributions (Figure 2).

Bone implants or bone grafts are widely used in the treatment of severe fractures or in tumor removal to replace a damaged or missing piece of bone. In order for the human body to accept the bone implant material and heal properly, it is essential that the bone implant be both mechanically and biologically compatible. Such implants can be made from various artificial bone materials, or from natural bone, in the form of allograft obtained from a donor, or an autograft taken from another bone of the patient. In any case, there arises the challenge of having correctly shaped implants created from an appropriate material, in a timely manner. Currently, during surgery, this challenge is met through the hand-shaping by the surgeon.

Even in the current era of sophisticated bone grafting procedures, advanced synthetic biomaterials and bioactive/tissue engineered implants, refined capabilities for restoring soft

tissue coverage, and highly evolved distraction osteogenesis techniques [30], treating segmental bone defects presents a major challenge. To date, most attention in this area has focused on mid-shaft long bone defects, where the principal reconstructive objective is to achieve bone healing with nominal preservation of limb length and alignment. While shape matching between the graft and the recipient site is always desirable in principle, many mid-shaft fractures are relatively forgiving in that regard. Various other bone defects, by contrast, place a much higher premium on close geometrical matching of the graft. For example, bone defects associated with severe articular or peri-articular fractures (i.e., fractures near a joint such as the knee or hip) require a substantially higher degree of reconstruction accuracy than is the case for the mid-shaft defects, owing to the need for stable, congruous articulation of the joint surface. Bone healing of an articular fracture in other than closely anatomic position predisposes the joint to secondary arthritis, a major contributing factor to poor outcomes, whose morbidity frequently approaches that of amputation [31].

At the local macroscopic level, all fractures possess individual geometric signatures. Current synthetic implant or grafting strategies for achieving healing of segmental defects offer only limited opportunity to address individualized defect geometry, since they have evolved mainly for situations (mid-shaft defects) where close reconstruction of local geometry is not particularly critical. Using conventional methods, there has to be primary reliance on fixation hardware to hold the respective bone surfaces in the desired nominal apposition, with the implant or graft making at best local spot contact with the recipient bone, and with appreciable gaps existing across much if not most of the intended-union interfaces. Even with the most advanced contemporary fixation in the hands of highly trained orthopaedic traumatologists, comminuted peri-articular fractures (especially in the presence of segmental defects) pose a severe biomechanical challenge, that often is not well resisted by usage of conventional bone grafts (Figure 3) [32]. Virtually all contemporary synthetic implant materials, all tissue engineered defect-filling constructs, and especially all variants of bone grafts would have better prospects for achieving optimal outcome if they began from a condition of closely fitting the local geometry of the recipient bone surface(s).

Although additive RP technologies provide the ability to create complex shapes in some biocompatible materials; other approved and desired materials are not usable, in particular, natural bone. Allograft bone holds strong preferential attraction over artificial biocompatible materials in many situations clinically [33,34]. However, two challenges need to be overcome in order to permit automated shape-machining of allograft bone. The first challenge is that, unlike engineered materials for which the source machining stock is in the convenient form of geometrically regular shapes such as cylinders or rectangular blocks, for allografts the source material is necessarily restricted to irregularly-shaped donor bones. The second prelude challenge is that, unlike for homogeneous artificial source materials for which the implant could be machined from anywhere arbitrarily within the original stock, for the case of donor bones the site and orientation of implant harvest need to respect the realities of heterogeneous internal bony architecture. From the clinical perspective, harvesting and creating implants from allograft bone still presents significant challenges.

To summarize, the previous research in this area leaves two related and somewhat dependent challenges, which provide the scope for this current work. One, the problem of

representing heterogeneous materials is generally not addressed sufficiently today. [Tissue banks normally do not collect CT density data for as-received donor bones, since this is very difficult to do under sterile condition.] Two, the more specific challenge of creating amorphous shaped heterogeneous components like bone implants is either unavailable or done completely by hand. To address these challenges, this paper first proposes an approach for compactly representing heterogeneous bony anatomy, and then a harvesting method that utilizes that approach to automate subtractive rapid prototyping of allograft bone implants working from CT scan data.

2. The *Matryoshka* Shell Model

This work proposes a novel way to create heterogeneous models of natural bone using a series of stacked shells. As such, the namesake "*Matryoshka*" is borrowed from the novelty Russian "nesting dolls." This stacked shell paradigm is used to describe the bone density distribution using discrete regions generated from normative CT image data. As a simple example, Figure 4(a) shows a set of Matryoshka nested dolls. The salient characteristic of Russian nesting dolls is that the size of each nested doll decreases in order to place one inside the other, as shown in Figure 4(b). Although models generated from bones will not always follow the monotonically decreasing regions of these dolls, the general concept of nested shells is appropriate for most long bones used to provide allografts (e.g., femurs, tibias, etc.).

The motivation behind the Matryoshka models used in this work is to provide a search space from within a proper harvesting site from which a bone implant can be found. This concept was shown in previous work focused on developing methods to create custom bone implants from donor bone, with implant geometries derived from CT scanning of bones [37]. The process of creating an implant begins with a CT scan of the fracture site, tumor resection site, etc., and then a computational reconstruction of the missing and/or unusable portion of bone. The resulting CAD geometry can be used in Subtractive Rapid Prototyping (SRP) to machine the implant from stock. Figure 5 shows a series of trial prototypes created using SRP on a variety of materials representing clinically relevant properties. The niche application of SRP lies in a relatively few materials, namely FDA-approved biomaterials like Trabecular Metal, or, of particular significance, natural allograft bone from a tissue bank. Allograft bone specifically motivates the need for a heterogeneous material modeling method; hence, it is the focus of this current work.

This work proposes using a simple method to evaluate and directly model the density of a given bone sample, namely through CT scanning. The Hounsfield Unit (HU), which indexes x-ray attenuation, indicates the varying levels of bone density; high HU corresponds to high density, and vice versa. HUs are also associated with grayscale of the CT slice image, which carries intensity information. By setting threshold HU values, pixel values below given threshold values can be identified as pixels-of-interest, while HU values above the threshold values can be identified as background pixels. Figure 6 shows an example of distinguishing pixels of interest from a CT slice image, using the HU threshold method. In this example, one can create different contours for each image. Hence, the CT slice image can be divided into five different regions bounded by different contours. When each increasing contour

shell is created, it is assumed that the pixels within that region have a common singular HU around the threshold value. In this manner, the continuous bone density function exhibited on the CT slice can be discretized into a step function. Straightforward extension of an iterative thresholding operation on a series of CT slices allows one to stack them together, and a 3D nested shell model can be created: the Matyroshka model.

An example of a Matryoshka model for a human tibia is shown in Figure 7. This model was constructed of five shells: an innermost medullary cavity shell (Shell 1), a low-density cancellous bone shell (Shell 2), a high-density cancellous bone shell (Shell 3), a cortical bone shell (Shell 4), and a bone outer surface (Shell 5). In this way, the entire 3D volume of the bone is classified as being within one of four bone regions, bounded by five shells. Although the general method applies for any surface model or polygonal file format, the present work uses the PLY file format. The PLY format was chosen for its ability to convey color information, which is not possible with the STL file format. Of course, the new Additive Manufacturing File Format (AMF) affords color, material, and much more information, and could be used instead of PLY formatting. However, even if an AMF file format were used, one would still need appropriate definitions of the material properties throughout the bone. As an alternative to doing this manually, a method is proposed here for creating the shells and automatically defining the material properties *a-priori*.

The major contribution of this approach is that the model can be automatically generated through an iterative process from a CT scan, rather than requiring manual construction by the user. In an additive manufacturing system, this might include assigning differing process parameters for each region, or simply choosing different material formulations. By contrast, the niche area of Subtractive Rapid Prototyping is particularly appropriate, where automatically planning for custom natural bone implants is the overarching challenge. Although previous research has applied rapid machining (CNC-RP) to fully automated process planning for industrial components [38–43], the challenge of rapid machining of natural bone begins with choosing a proper “harvesting” location from which to extract the bony geometry of the implant from within the donor bone. In other words, one is faced with the challenge of finding a suitable location from which to machine an arbitrary free-form shaped object from within another arbitrary free-form shaped stock material object, where each has a unique material density distribution. Figure 8 illustrates an example of this type of implant harvest. Figure 8(a) shows the CT-derived CAD model of the desired implant (with added holes for fixation screws), while Figure 8(b) shows a surrogate bone human tibia. Lastly, Figure 8(c) shows the “harvest” location, where it was deemed best to machine the implant from within the donor bone, based on geometry and density distribution.

Identifying desired implant geometry is facilitated by unique “3D puzzle solving” algorithms and software, which can create accurate 3D CAD model reconstructions of the missing bone directly from CT scan data [44]. This software was originally developed to reassemble a fracture site (i.e., locating and aligning all the puzzle pieces in their proper anatomic position). However, it became apparent that Boolean operations on the “puzzle” solution, compared to a mirrored image of the intact “other” limb (right or left), could reveal the correct geometry of any missing pieces, as well.

The following sections provide an approach to search and evaluate potential implant harvest sites from within a donor bone using a Matryoshka shell model. The goal is to automatically define the "goodness" of a location using quantifiable metrics. Currently, an overall bone *Density* score and/or a *Similarity* score are used to provide best locations to achieve highest density and best-matching density distributions, respectively.

Using a Matyroshka model for bone implant harvesting

As a practical matter, human *long bones* (femur, tibia, humerus, etc.) are most attractive as donor bones. Long bones generally have a hard outer surface of compact bone, a spongy inner region comprised of cancellous bone, and bone marrow. If one considers the shape similarity between a long bone and a cylinder, a long bone generally exhibits increasing density as one moves away from the axis radially, or, away from the medullary canal in the center of the bone. This gives a basis for defining the "center line" of the bone.

It is assumed that both patient bone and donor bone have already been aligned approximately anatomically such that the *anterior*, *posterior*, *proximal*, *distal*, etc. directions correspond to standard views. This assumption is based on experience with medical imaging, whereby radiologists set orientations and describe views in standardized "coordinate systems," not unlike the way CAD modelers use the terms "front," "right," and "side" views in orthogonal projections.

Before initiating a search for the harvest location within the donor bone, an important first step is to align the "center lines" or axes of the patient bone and donor bone. Thus, the distributions of density in the implant and the donor bone would generally align radially along the same axis. As such, when one traverses a set of cylindrical coordinates in the donor or patient bone space, the gradient directions would generally align (i.e. moving away radially will increase density in both, and vice versa).

The procedure of identifying the "center line" of the donor bone involves straightforward slicing of the shaft of the donor bone and patient bone models. Next, using a least squares method, we fit the centroids of the chains on all of the slices with a linear function (straight line). The straight line is approximated as the "center line" of the donor and patient bones. Next, both bones are aligned to a common *Z*-axis orientation (Figure 9). At this point, both donor and patient bones are in the same orientation (Figure 9(a)), and although they do not lie on the same axis, they need a common final alignment. Achieving this is simply a matter of uniaxial translation so as to align the ends of the patient and donor bones (Figure 9(b)). Next, the implant geometry is translated into the donor bone space in order to start evaluating possible harvest positions (Figure 9(c)).

Searching for the best harvest location involves rotating the implant around the center line of the donor bone, and translating the implant along the center line axis direction and radially toward and away from the center line. Note that the implant is not initially located at the "same" rotation about the centerline axis from where it originated in the patient. The following sections describe an exhaustive search process, demonstrating why this is unnecessary.

Creating a discretized slice model

Before the iterative search begins, the space available for potential implant harvesting is discretized through a process enabled by the Matryoshka model. A key characteristic of the Matryoshka strategy is that the 3D space is reduced to simpler, yet still highly detailed slice information (i.e. the color slice image in Figure 10(a)). The color slice can be considered as a "boundary"; the region within each color boundary is assigned a specific value, representing its density. In this manner, all elements contained between two adjacent shells are set to the same value, other than the first shell, which only contains the medullary canal and is not a feasible region for bone harvesting. As shown in Figure 10(b), values *a*, *b*, *c*, and *d* represent the bone densities from different regions in the slice model, whereby the continuously varying bone density is discretized into four different regions on the slice that are available as potential harvesting locations. Next, a spider cell structure is used to discretize each slice into a grid of sectors about the *Z*-axis, with an interval angle α, and with each sector further divided by grid elements with interval *h*, as shown in Figure 10(c). Each grid element is assigned a specific value indicating the density of the region encompassed by the corresponding grid element. In general, smaller α and *h* will result in a more accurate and finer discretization structure, but at the expense of increased computation time (the grid spacing for both α and *h* are shown excessively coarse in Figure 10(c) for clarity; in practice, they are 1–5° and 1–3 mm, respectively).

For each slice, an array is used to indicate the presence of the shell in the grid structure (Figure 11(a)). If any side of the grid element intersects the slice chain, a specific value is assigned to represent the existence of a specific shell in that element at a specified density, with values of *a*, *b*, *c*, and *d* used to represent the existence of Shell 2, Shell 3, Shell 4 and outer surface Shell 5, respectively. If no shell intersects any grid element, a value of 0 is assigned to the corresponding element in a 2D array as shown in Figure 11(b).

Since all grid elements that fall within the surface boundaries of the bone will be assigned to one of the specific density regions, those grid elements temporarily indexed in the array with a value of 0 must be modified to represent the density correctly. For example, after filling in the 0 elements of the array, the updated row of the array is shown in Figure 11(b).

Density score and similarity score calculation

The goal is to assign a quantitative score of "goodness" for a candidate location for bone harvesting. This will involve the density of the implant, regardless of whether the preference is simply for high overall density, or for a highly similar distribution of densities between donor and patient. So, after discretizing the slice model into the grid structure and assigning a density value in each element, the area of each element is determined based on parameters α and *h*. Only those elements which are inside of the implant slice chains or which contain implant slice chains are used to calculate the implant density score, as shown in Figure 12.

To calculate the overall effectiveness score for the entire provisional implant position, density metrics are calculated for each chain of each slice for the entire implant, as follows.

Let *N* be the total number of slices for the implant, for *i* slices from 0 to $N-1$. Let *j*, ranging from 0 to 3, represent the four bone density regions. Then, let S_{ij} indicate the area of the

different density regions *j* on slice *i*. Recall that the density regions 0, 1, 2, 3 represent the range from low-density cancellous bone region to the highest density cortical bone region. Then, the area matrix *S* is normalized by:

$$S_{ij}=\frac{S_{ij}}{\sum_{i=0}^{N-1}\sum_{j=0}^{3}S_{ij}} \quad (1)$$

i=0, 1,… (*N*−1) (slice), *j* = 0, 1,…, 3 (region)

Finally, the density score is calculated by:

$$Density\ score=\sum_{i=0}^{N-1}\sum_{j=0}^{3}(S\times A^{T}) \quad (2)$$

$$A=[a,b,c,d] \quad (3)$$

Using the same procedure, the normalized area matrices *S* and *S*’ are calculated for the donor bone and patient bone, respectively. The similarity score is then calculated by:

$$Similarity\ score=\sum_{i=0}^{N-1}\sum_{j=0}^{3}abs(S_{ij}-S'_{ij}) \quad (4)$$

These two scores, *Density* and *Similarity*, can then be used independently or together, to calculate the effectiveness of a provisional harvest site. Whereas *Density* is an aggregate score for the entire implant, *Similarity* is evaluated slice by slice. Hence, although one could achieve a high overall *Density* score by having some portion of the implant gain density at the expense of another portion losing density, the *Similarity* score will be affected more locally.

Conceptually, the simplest approach is to conduct an exhaustive search of the entire donor bone space to determine the optimal location for the harvested implant. This exhaustive search involves rotating the implant about the *Z*-axis and translating the implant up and down in the *Z*-axis direction, all while moving the implant closer to or farther from the *Z*-axis radially. In other words, the implant is moved at the granularity of the spider grid structure throughout the entire donor bone space. For each iteration, the *Density* and *Similarity* are calculated, and then both values are normalized. In our current implementation, a final attractiveness score is calculated based on a weighted function of the aggregate “goodness” of each feasible solution.

$$Max\{\alpha\times Normalized(Density\ score)+\beta\times Normalized(Similarity\ score)\} \quad (5)$$

Here α and β are coefficient weights on the importance of *Density* and *Similarity*; these are values which can be assigned by the surgeon, radiologist, tissue bank technician, etc.

3. Implementation example

Matryoska model generation and harvesting search

The algorithms developed in this work have been implemented in C++ and are graphically displayed using *OpenGL*. To illustrate the implementation of these analyses, two sets of human tibia bone CT scan slices are used. These slices were first imported into ITKsnap (open source software) and saved as a voxel array DICOM file. Next, the DICOM data were loaded into MATLAB, and the five Matyroshka shells were generated using an increasing Hounsfield Unit cutoff. The created shells were then saved into a PLY file in MATLAB, and imported to RapidForm software for post-processing. Post-processing included correcting the geometric errors in the PLY file (holes, spikes, etc.). The post-processed shells created were the marrow canal (Shell 1), one lower-density cancellous bone (Shell 2), one higher-density cancellous bone (Shell 3), the cortical bone shell (Shell 4) and the outer tibia surface (Shell 5), as shown in Figure 13, listed with the respective HU used to generate them.

One set of the CT scan images had 566 slices, each of 228×264 voxels and within spacing of 0.3 mm. The other set of data had 298 slices of 205×298 voxels, within spacing of 0.5 mm. From each set of CT scan images, a polyhedral PLY file was generated. These PLY files were subsequently used for harvesting analysis. Both patient bone and donor bone models were sliced with 2.0 mm spacing. To create the "spider," discretization parameters α and h were chosen to be 3° and 1.35 mm, respectively. The overall *Density* score of the implant from within the original patient bone was found to be 435.

It is worth noting that there are two goals in the implementation, or at least, two modes of use envisioned. Although the methods in this paper allow direct investigation of the total numerical scores and optimization, surgeons may in fact desire a tool to manipulate implant sites by hand so as to receive a real-time score for each provisional harvest position. Conceptually this would take the form of an "applause meter," which gives the surgeon feedback during manipulation of the implant in the design space.

Based on this second implementation concept, an initial interactive graphics software interface has been developed (Figure 14). In this example, after aligning the ends of patient bone and donor bone, the implant was translated into the donor bone, where the initial *Density* score and *Similarity* score of the harvested implant in the donor bone were found to be 339 HU and 1, respectively. In Figure 14(a), the black arrow pointing to the left color bar shows the *Density* score of the implant in the original patient bone, while the pink arrow pointing to the right color bar shows the *Density* score of the harvested implant from within the donor bone. Likewise, the pink arrow pointing to the right color bar represents the *Similarity* score (There is obviously no "original" similarity to compare against). After rotating the implant about the *Z*-axis by 103°, translating the implant along the *Z*-axis direction by −4.0 mm, and moving the implant radially by 1.0 mm, the updated *Density* score and *Similarity* scores of the harvested implant in the donor bone are 533 HU and 1, respectively. In Figure 14(b), we note that the pink arrow pointing to the *Density* bar jumps above the black arrow, which denotes that the new provisional harvested location has a higher *Density* score than the original implant within the patient bone. In this case, the *Similarity* score remained essentially the same.

We envision a surgeon using an interactive tool to move the implant around the donor bone and monitor the *Density* and *Sensitivity* bars to aid in finding a best site for harvesting. The ideal for the allograft in most instances would be to replicate the normal native local density distribution of bone at the recipient site. However, the program would also allow the requesting surgeon to over-ride that default condition, by prescribing a desired density distribution of his/her choosing as clinical indications dictate. Under cursor control, the tissue bank operator would then provisionally position the idealized allograft geometry at a plausibly acceptable location within the donor bone geometry. Given the goodness-of-match between the provisional harvest and the idealized allograft HU distributions, and given the degree of acceptability of the structural stiffness of the corresponding provisional sacrificial supports, the overall attractiveness of that provisional harvest position would then be quantitatively scored, and feedback provided to the operator. The benefits of this new software, which would be most helpful from the clinical perspective, would be both the user-friendly real-time interface, as well as ability of the software to choose a best fit for both geometry and density. Currently available software provides no basis (other than operator judgment) for selecting the specific harvest site beyond ensuring that the implant object to be machined lies entirely within the outer surface of the donor bone. The following presents an implementation of an automated search for a harvest location using the developed models.

To conduct an automated search for our implementation, we iterated through the design space and recorded results for *Density* and *Similarity*. Through rotations of the implant about the *Z*-axis by 3° increments, translating the implant along the *Z*-axis direction in 2 mm increments, and moving the implant radially by 1.5 mm increments, we generated the normalized *Density* score and *Similarity* score plots for several donor bone models. As one example, Figure 15 shows a plot of Density scoring for one sample bone, where maximal value is achieved at iteration 2,575.

Implant Harvesting using CNC-RP

CNC-RP is a fully automated Subtractive Rapid Prototyping process that uses a 3-axis vertical milling machine with a 4^{th} axis indexer for multiple setup orientations [Frank *et al.*, 2006, 2007]. In this system, round stock material is fixed between two opposing chucks and rotated between operations using the indexer, and visibility analysis of cross sectional slice data provides a basis for automated setup planning about a single axis. This implementation uses a modified Greedy set cover algorithm to determine orientations. For each orientation, all visible surfaces are machined using simple layer-based toolpath planning while leaving a structure of “sacrificial supports” that are used to fixture the part (keeping the part attached to the remainder of the stock). The number of rotations required to machine a model is dependent upon its geometric complexity. Once all of the operations are complete, the supports are severed in a final series of operations, and the part is removed. Figure 16 illustrates the process steps for creating a typical complex part using this strategy.

The motivation for the Matryoshka model and harvesting search method has been to determine a solution for optimal “harvesting” when using Subtractive Rapid Prototyping (CNC-RP) for custom bone implants. To illustrate that the Matryoshka approach can be used

to plan harvesting locations for creating a custom bone implant from a donor bone, an example of harvesting an implant using CNC-RP is demonstrated. The approach starts with scanning a surrogate potted tibia bone, as shown in Figures 17(a) and 17(b). The Matryoshka model was used to find the best position and orientation within the donor bone from which to harvest the implant, as shown in Figure 17(c). Following the determination of the implant harvest location, the corresponding region from the bone was cut and used as machining stock for further process planning. Figures 17(d) and (e) show the bone cut section. The locations for the sacrificial supports on the implant were determined by the CNC-RP software, and are shown in Figure 17(f). Figure 17(g) demonstrates the CAD model of a cut section with the support in it.

We have developed a device to implement a procedure for physically machining arbitrarily-shaped implants from within irregular donor bone geometries. Given a desired implant shape, a specific donor bone, a desired position and orientation from within the donor bone from which the implant is to be harvested, the essential problem is to position the donor bone in such a manner that sacrificial supports can be passed in appropriate orientations through the donor bone, terminating at locations that will be just inside the to-be-harvested implant. The setup used for this purpose is shown in Figure 18(a). The donor bone is temporarily (manually) screw-affixed to a base plate, at one of an array of alternative locations. The disk templates are then registered relative to the base plate in positions such that a desired number (minimum of two per disk) of the sacrificial supports can be passed so as to intersect the desired implant surfaces - Figure 18(b). After drilling holes and embedding the sacrificial supports to the necessary depths, the bone, disk, and support units are removed *en bloc* from the base plate and positioned within the 4-axis milling machine - Figure 18(c). Figures 18(d) and (e) show the implant machining from different angles. The finished implant is demonstrated in Figure 18(f). The original implant CAD model and machined implant with supports removed are shown in Figures 18(g) and (h).

Complete processing of an implant can be done in a matter of hours. As presently implemented, the harvest site search process takes approximately 20 minutes. The SRP software requires approximately 15–30 minutes to automatically generate all setups, supports, and toolpaths. Finally, the total processing time is on the order of a few hours. This overall time period is consistent with the goal of delivering a custom implant within a few days of a traumatic incident; most surgeries for extreme trauma involve waiting several days for physiologic stabilization, reduction in swelling, etc.

4. Conclusion

This paper presents a new method for multi-material model representation using nested polygonal shells, analogous to a Matryoshka doll. Compared with methods of hand-creating an assembly model for input to a multi-material additive RP system, this method could potentially be completely automated, given a set of parameters. This work illustrates how the Matryoshka model can be used to plan harvesting locations for creating custom bone implants from within actual human donor bones, and it develops an approach to calculate a *Density* score and *Similarity* score for an arbitrary provisional implant harvest site, to evaluate the overall effectiveness of that harvest site.

This approach to finding the optimal implant harvest site within a donor bone still leaves room for improvement, and is not necessarily a generic solution for all multi-material components. The method has, however, proven effective for human long bones, which can be approximated by a cylinder model. In these bones, it is relatively easy to find the center line, and it is reasonable to assume that the density of the long bone decreases from the outer surface to the center line. Based on this assumption, the implant is simply rotated around the center line. If the bone is not a long bone, and/or cannot be approximated as a cylinder, one would need to allow the implant to “tumble” in 3D space. Hence, an exhaustive search would probably not be tractable since the solution space would be much larger. Future work with the Matryoshka approach could be used to develop a better harvesting solution for irregular and/or flat bones. It could also be used to pursue variants of the method for use in industrial components which may have less amorphous shapes, and which could be printed using existing additive systems such as LENS or polyjet printing.

Acknowledgments

This work was supported by grants from the NIH/NIAMS (P50AR055533 and R21AR054015), the Roy J. Carver Charitable Trust at the University of Iowa, State of Iowa Economic Development appropriations to the Board of Regents under the Grow Iowa Values Fund and the Musculoskeletal Transplant Foundation. The authors would also like to recognize the technical support of Mr. Gary Ohrt and Dr. Thad Thomas at the University of Iowa..

References

1. Kumar V, Burns D, Dutta D, Hoffmann C. A framework for object modeling. Computer-Aided Design. 1999; 31(9):541–556.
2. Markworth AJ, Ramesh KS, Parks WP. Modeling studies applied to functionally graded materials. Journal of Materials Science. 1995; 30(9):2183–2193.
3. Kruth JP, Mercelis P, Vaerenbergh JV, Froyen L, Rombouts M. Binding mechanisms in selective laser sintering and selective laser melting. Rapid Prototyping Journal. 2005; 11(1):26–36.
4. Harrysson OLA, CansiZoglu O, Marcellin-Little DJ, Cormier DR, West HA. Direct metal fabrication of titanium implants with tailored materials and mechanical properties using electron beam melting technology. Materials Science &Engineering.C, Biomimetic Materials, sensors and systems. 2008; 28(3):366–373.
5. Thomsen P, Malmström J, Emanuelsson L, René M, Snis A. Electron beam-melted, free-form-fabricated titanium alloy implants: material surface characterization and early bone response in rabbits. Journal of Biomedical Materials Research Part B Applied Biomaterials. 2009; 90(1):35–44.
6. España FA, Balla VK, Bose S, Bandyopadhyay A. Design and fabrication of CoCrMo alloy based novel structures for load bearing implants using laser engineered net shaping. Materials Science and Engineering: C. 2009; 30(1):50–57.
7. Bandyopadhyay A, Krishna BV, Xue W, Bose S. Application of Laser Engineered Net Shaping (LENS) to manufacture porous and functionally graded structures for load bearing implants. Journal of Materials Science: Materials in Medicine. 2009; 20(1):s29–s34. [PubMed: 18521725]
8. Balla VK, Bodhak S, Bose S, Bandyopadhyay A. Porous tantalum structures for bone Implants: fabrication, mechanical and in vitro biological properties. Acta Biomater. 2010; 6(8):3349–3359. [PubMed: 20132912]
9. Williams, CB.; Mistree, FM.; Rosen, DW. Investigation of solid freeform fabrication processes for the manufacture of parts with designed mesostructure; ASME IDETC Design for Manufacturing and the Life Cycle Conference; 2005. DETC2005/DFMLC-84832.
10. Wang, H.; Johnston, SR.; Rosen, DW. The Seventeenth Solid Freeform Fabrication Symposium. Austin, TX: 2006. Design of a graded cellular structure for an acetabular hip replacement component; p. 111-123.

11. Kou XY, Tan ST. Heterogeneous object modeling: A review. Computer-Aided Design. 2007; 39(4):284–301.
12. Chen M, Tucker JV. Constructive volume geometry. Computer Graphics Forum. 2000; 19(4):281–293.
13. Chandru V, Manohar S, Prakash CE. Voxel-based modeling for layered manufacturing. Computer Graphics and Applications, IEEE. 1999; 15(6):42–47.
14. Jackson, T. Ph.D. thesis. Massachusetts Institute of Technology; 2000. Analysis of functionally graded material object representation methods.
15. Shin KH, Dutta D. Constructive representation of heterogeneous objects. Journal of Computing and Information Science in Engineering. 2001; 1(3):205–217.
16. Zhu, F. M.Phil. thesis. The University of Hong Kong; 2004. Visualized CAD modeling and layered manufacturing modeling for components made of a multiphase perfect material.
17. Elishakoff I, Gentilini C, Viola E. Three-dimensional analysis of an all-round clamped plate made of functionally graded materials. Acta Mechanica. 2005; 180(1–4):21–36.
18. Siu YK, Tan ST. 'Source-based' heterogeneous solid modeling. Computer-Aided Design. 2002; 34(1):41–55.
19. Biswas A, Shapiro V, Tsukanov I. Heterogeneous material modeling with distance fields. Computer Aided Geometric Design. 2004; 21(3):215–242.
20. Liu H, Maekawa T, Patrikalakis NM, Sachs EM, Cho W. Methods for feature-based design of heterogeneous solids. Computer-Aided Design. 2004; 36(12):1141–1159.
21. Samanta K, Koc B. Feature-based design and material blending for freeform heterogeneous object modeling. Computer-Aided Design. 2005; 37(3):287–305.
22. Qian X, Dutta D. Design of heterogeneous turbine blade. Computer-Aided Design. 2003; 35(3): 319–329.
23. Pasko A, Adzhiev V, Schmitt B, Schlick C. Constructive hypervolume modeling. Graphical Models. 2001; 63(6):413–442.
24. Yao J, Taylor R. Construction and simplification of bone density models. Proceedings of SPIE. 2001; 4322:814–823.
25. Bibb R, Sisias G. Bone structure models using Stereolithography: a technical note. Rapid Prototyping Journal. 2002; 8(1):25–29.
26. Chen ZZ, Li DC, Lu BH, Tang YP, Sun ML, Wang Z. Fabrication of artificial bioactive bone using rapid prototyping. Rapid Prototyping Journal. 2004; 10(5):327–333.
27. Fang Z-B, Starly B, Shokoufandeh A, Regli W, Sun W. A computer-aided multi-scale modeling and direct fabrication of bone structure. Computer-Aided Design and Applications. 2005; 2(5): 627–634.
28. Sun W, Starly B, Darling A, Gomez C. Computer-aided tissue engineering: application to biomimetic modeling and design of tissue scaffolds. Biotechnology and Applied Biochemistry. 2004; 39(1):49–58. [PubMed: 14556653]
29. http://academic.uofs.edu/faculty/kosmahle1/courses/pt245/trabecul.htm.
30. Nauth A, McKee MD, Einhorn TA, Watson JT, Li R, Schemitsch EH. Managing bone defects. J Orthop Trauma. 2011; 25(8):462–466. [PubMed: 21738065]
31. Bosse MJ, MacKenzie EJ, Kellam JF, Burgess AR, Webb LX, Swiontkowski MF, Sanders RW, Jones AL, McAndrew MP, Patterson BM, McCarthy ML, Travison TG, Castillo RC. An analysis of outcomes of reconstruction or amputation after leg-threatening injuries. New Engl J Med. 2002; 347(24):1924–1931. [PubMed: 12477942]
32. Vallier HA, Hennessey TA, Sontich JK, Patterson BM. Failure of LCP condylar plate fixation in the distal part of the femur - A report of six cases. J Bone Joint Surg Am. 2006; 88(4):846–853. [PubMed: 16595476]
33. Skendzel JG, Sekiya JK. Arthroscopic glenoid osteochondral allograft reconstruction without subscapularis takedown: technique and literature review. Arthroscopy. 2011; 27:129–135. [PubMed: 21187250]

34. Clowers BE, Myerson MS. A novel surgical technique for the management of massive osseous defects in the hindfoot with bulk allograft. Foot and Ankle Clinics. 2011; 16:181–189. [PubMed: 21338938]
35. http://www.thefoxisblack.com/2009/12/07/matte-black-nesting-dolls-by-muji/.
36. http://geekopedia.blogspot.com/2009/04/munecas-rusas.html.
37. Frank, MC.; Hunt, CV.; Anderson, DD.; McKinley, TO.; Brown, TD. Proceedings of the Solid Freeform Fabrication Symposium. Austin TX: 2008 Aug. Rapid manufacturing in biomedical materials: using subtractive rapid prototyping for bone replacement; p. 686-696.
38. Frank MC, Wysk RA, Joshi SB. Determining setup orientations from the visibility of slice geometry for rapid CNC machining. Journal of Manufacturing Science and Engineering. 2006; 128(1):228–238.
39. Li Y, Frank MC. Machinability analysis for 3-axis flat end milling. Journal of Manufacturing Science and Engineering, Transactions of the ASME. 2006; 128(2):454–464.
40. Li Y, Frank MC. Computing non-visibility of convex polygonal facets on the surface of a polyhedral CAD model. Computer Aided Design. 2007; 39(9):732–744.
41. Frank, MC. Proceedings of the Solid Freeform Fabrication Symposium. Austin, TX: 2007. Implementing Rapid Prototyping using CNC machining (CNC-RP) through a CAD/CAM interface; p. 112-123.
42. Boonsuk W, Frank MC. Automated fixture design for a rapid machining process. Rapid Prototyping Journal. 2009; 15(2):111–125.
43. Petrzelka EJ, Frank MC. Advanced process planning for subtractive rapid prototyping. Rapid Prototyping Journal. 2010; 16(3):216–224.
44. Thomas TP, Anderson DD, Willis AR, Liu P, Marsh JL, Brown TD. Virtual pre-operative reconstruction planning for comminuted articular fractures. Clinical Biomechanics. 2011; 26(2): 109–115. [PubMed: 21215501]
45. http://fpnotebook.com/ortho/Anatomy/FmrBn.htm.

Biographies

Shuangyan Lei is a PhD candidate in Industrial Engineering at Iowa State University. She received her BS (2006) in Electrical Engineering from Xidian University and MS (2010) in Mechanical Engineering from the Iowa State University. Her research interest is in the area of manufacturing. She is a recipient of the ISU Research Excellence Award in 2010.

Matthew C. Frank, PhD is an Associate Professor in the Department of Industrial and Manufacturing Systems Engineering at Iowa State University. Dr. Frank earned his BS and MS in Mechanical Engineering and a PhD in Industrial Engineering from Penn State University. His research and teaching interests involve the general area of manufacturing, with a specific focus on rapid manufacturing and prototyping. He has published numerous papers and book chapters on RP and other manufacturing topics, has received the ISU E-Week Outstanding Professor Award for 2005 and the 2006 SME Outstanding Young Manufacturing Engineer Award and currently holds one US patent. Matthew C. Frank is the corresponding author and can be contacted at: mfrank@iastate.edu

Donald D. Anderson, PhD is an Associate Professor at the University of Iowa in the Department of Orthopaedics and Rehabilitation, with a secondary appointment in Biomedical Engineering. Anderson holds a BSE in Biomedical Engineering, as well as an MS and a PhD in Mechanical Engineering (Biomechanics emphasis). During his over 20 years of post-doctoral professional experience, Anderson’s primary research focus has been in articular joint biomechanics, specifically investigating the relationship between joint

injury and subsequent development of post-traumatic OA. Anderson is currently President of the American Society of Biomechanics and also a member of the American Society of Mechanical Engineers, the Orthopaedic Research Society, the Orthopaedic Trauma Association, the Osteoarthritis Research Society International and the International Society of Biomechanics.

Thomas D. Brown, PhD, is the Richard and Janice Johnston Chair of Orthopaedic Biomechanics at the University of Iowa, where he holds faculty appointments in the Departments of Orthopaedics and Rehabilitation (primary), Biomedical Engineering (secondary) and Mechanical Engineering (courtesy). His PhD (1976) is from Carnegie-Mellon University, in Mechanical Engineering – Bioengineering. Brown's research interests are in orthopedic biomechanics and in clinical biomechanics of the musculoskeletal system. He is a past president of the American Society of Biomechanics and of the Orthopaedic Research Society and currently serves as Deputy Editor for Research of the *Journal of Bone and Joint Surgery*.

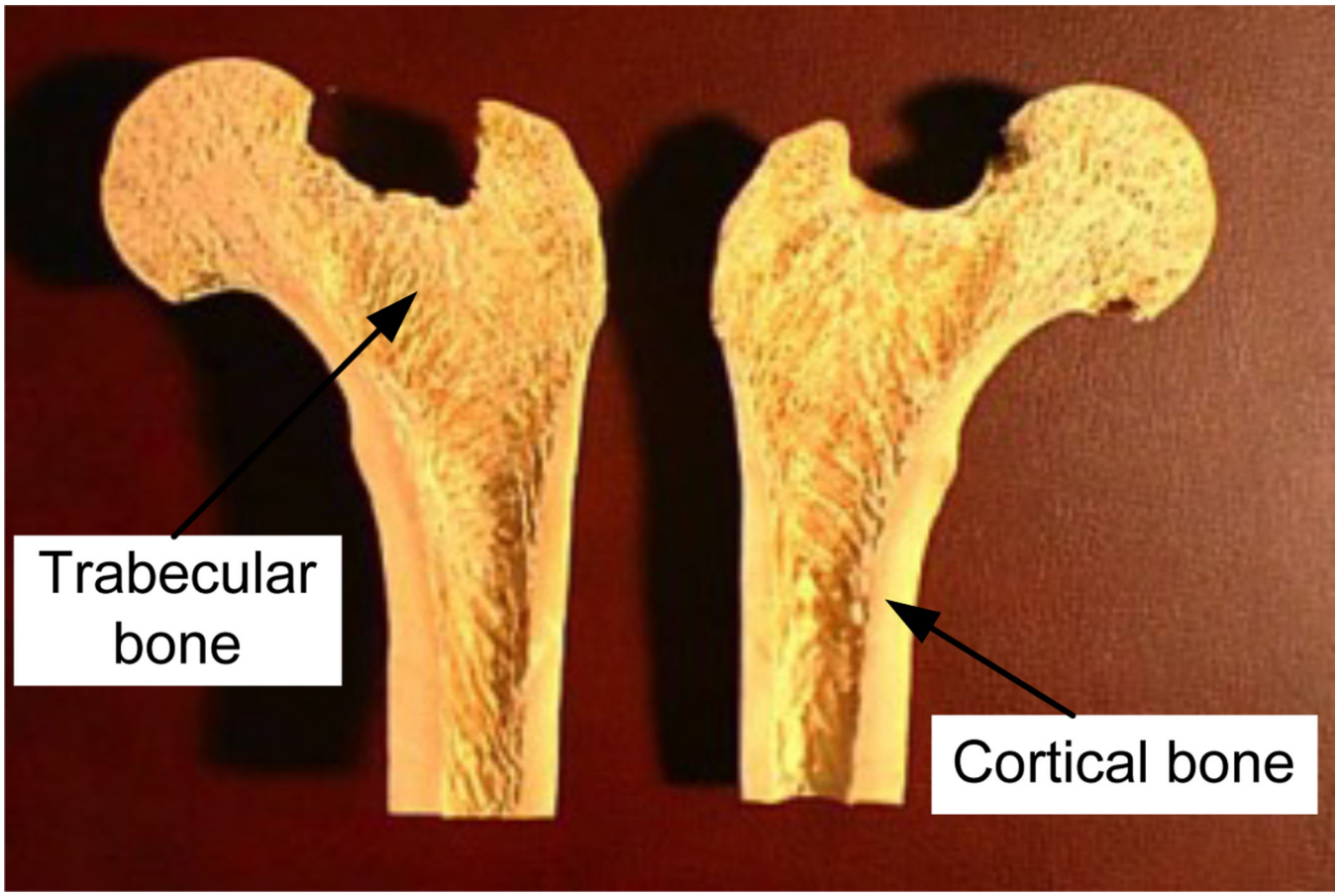

Figure 1.
A cross-sectional view of a femur bone.

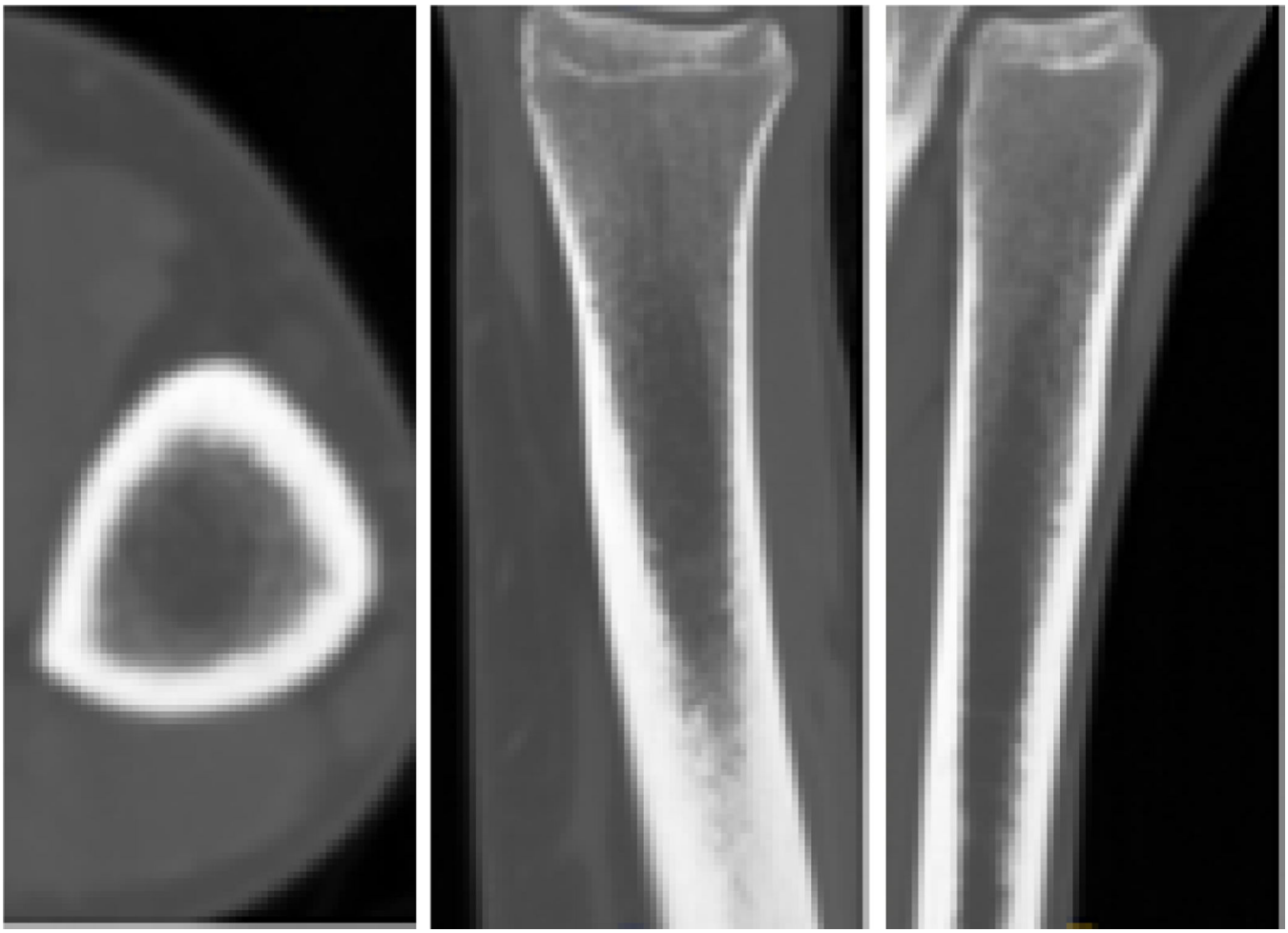

Figure 2.
CT slices along different axes[29].

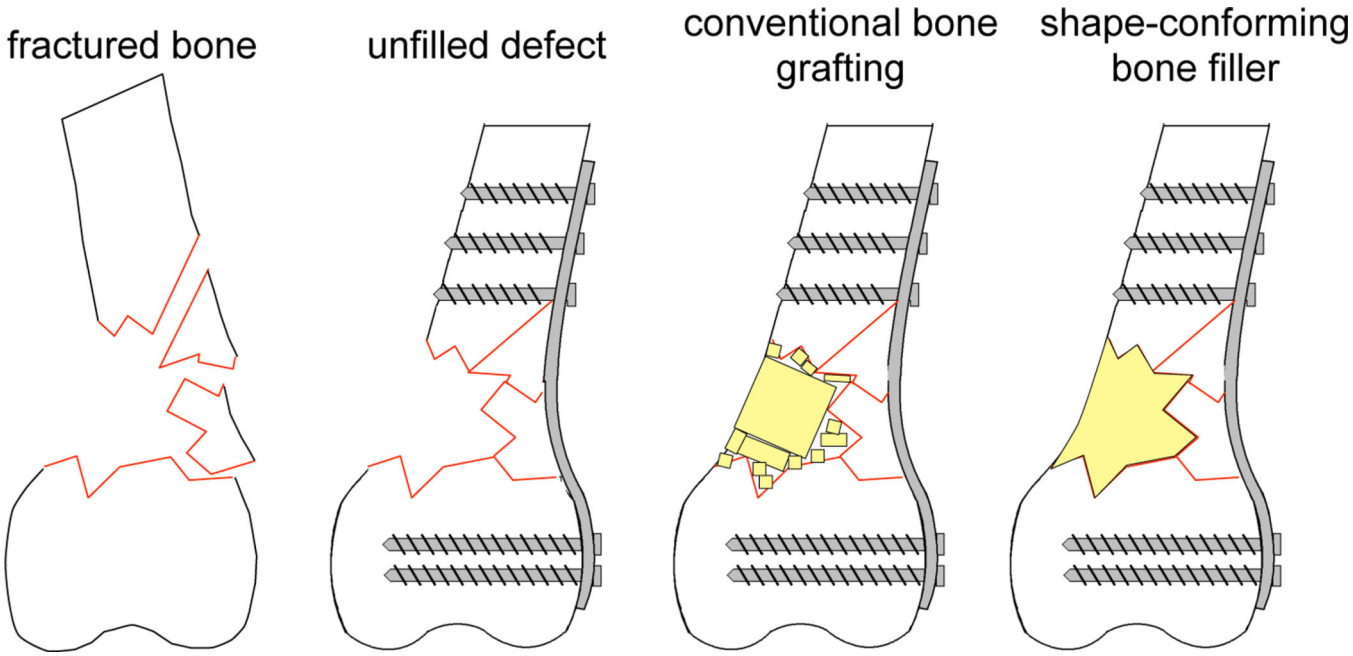

Figure 3.
Schematic of a typical fracture with different options shown.

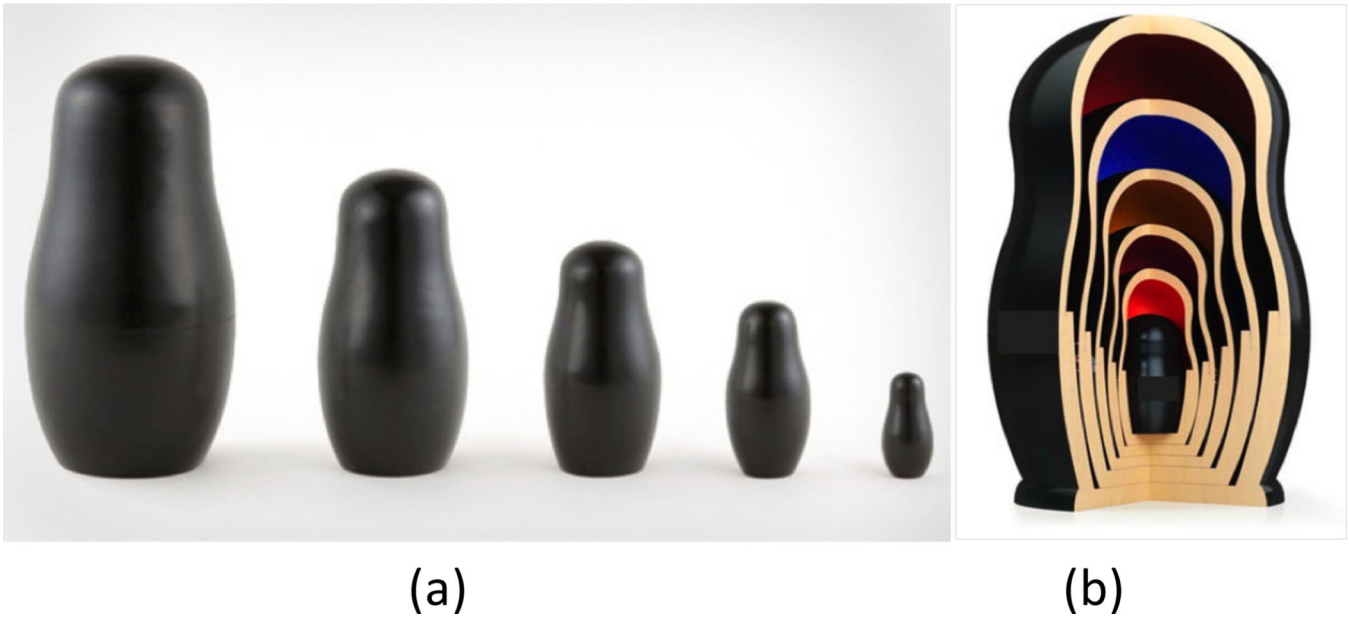

Figure 4.
Matryoshka shell model. (a) Set of Matryoshka dolls, in order of size [35] and (b) Cut-away view of nested Matryoshka dolls [36].

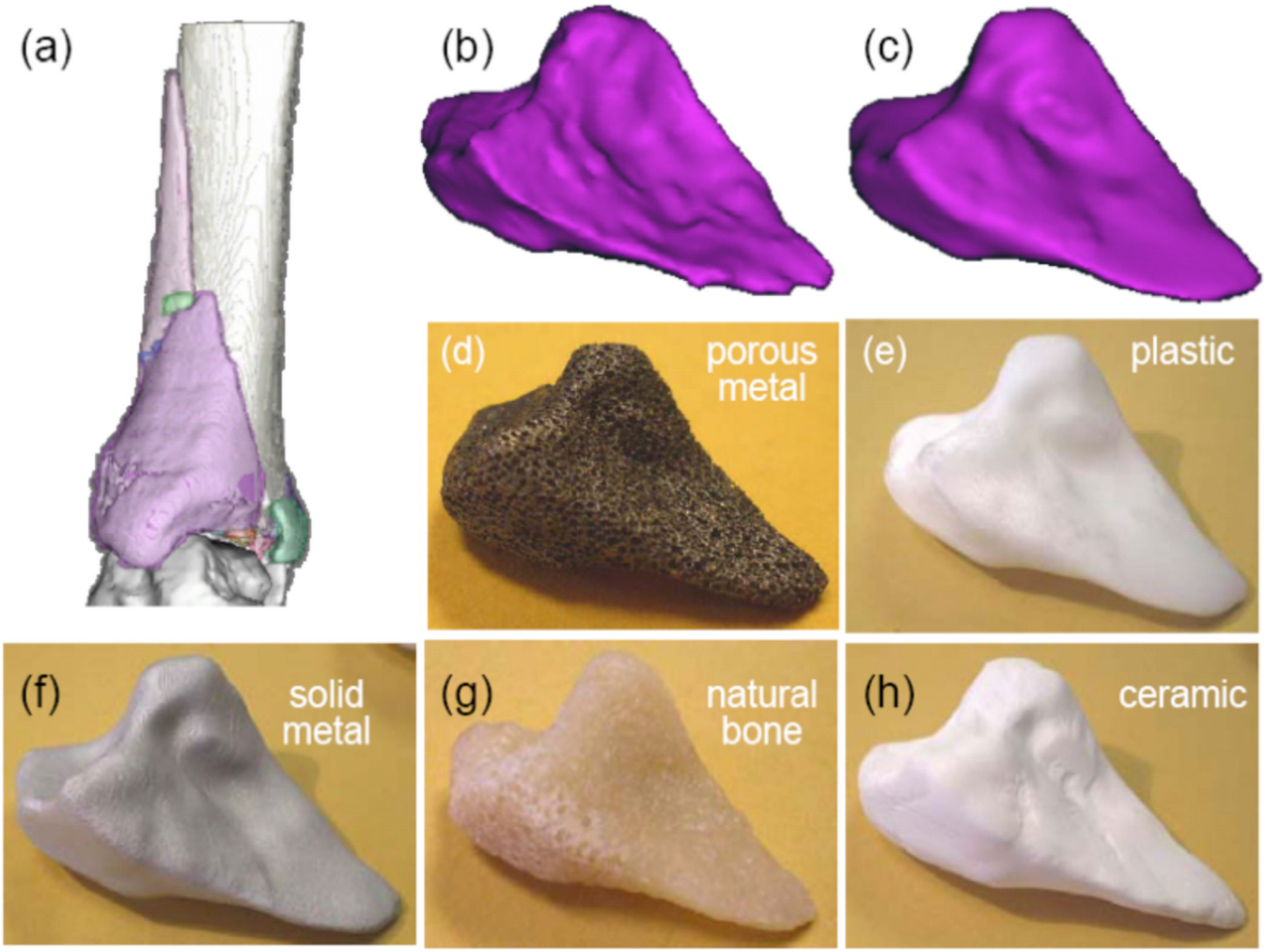

Figure 5.

Sample implant materials from a variety of clinically relevant materials. (a) Segmented CT image showing various fragments; (b) Individual computational fragment image as extracted, and (c) as computationally smoothed; (d–h) Corresponding 3D fragment geometries created using SRP from Trabecular Metal®, plastic, solid metal, bovine bone, and porous ceramic.

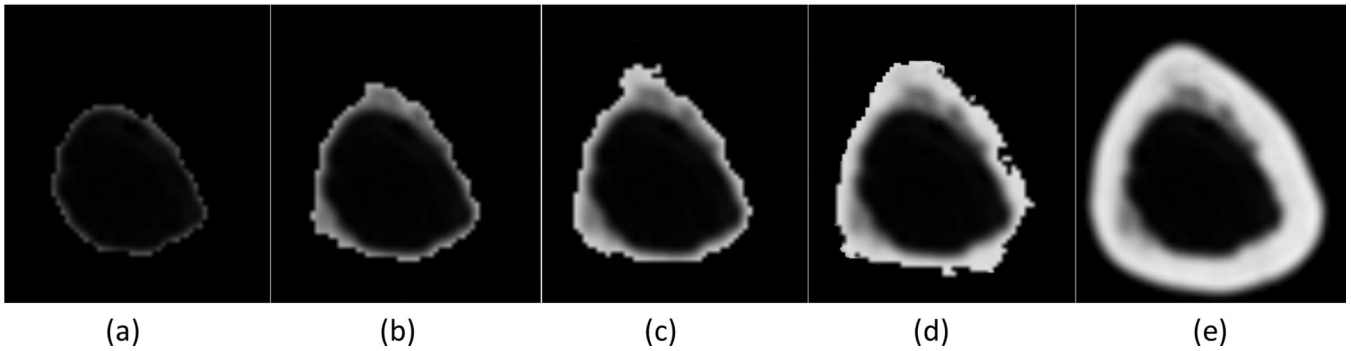

Figure 6.

Distinguishing the pixels of interest from the CT slice image by the HU threshold method. (a) HU ≤1203; (b) HU ≤2277; (c) HU≤2768; (d) HU≤2982; (e) HU ≤3140.

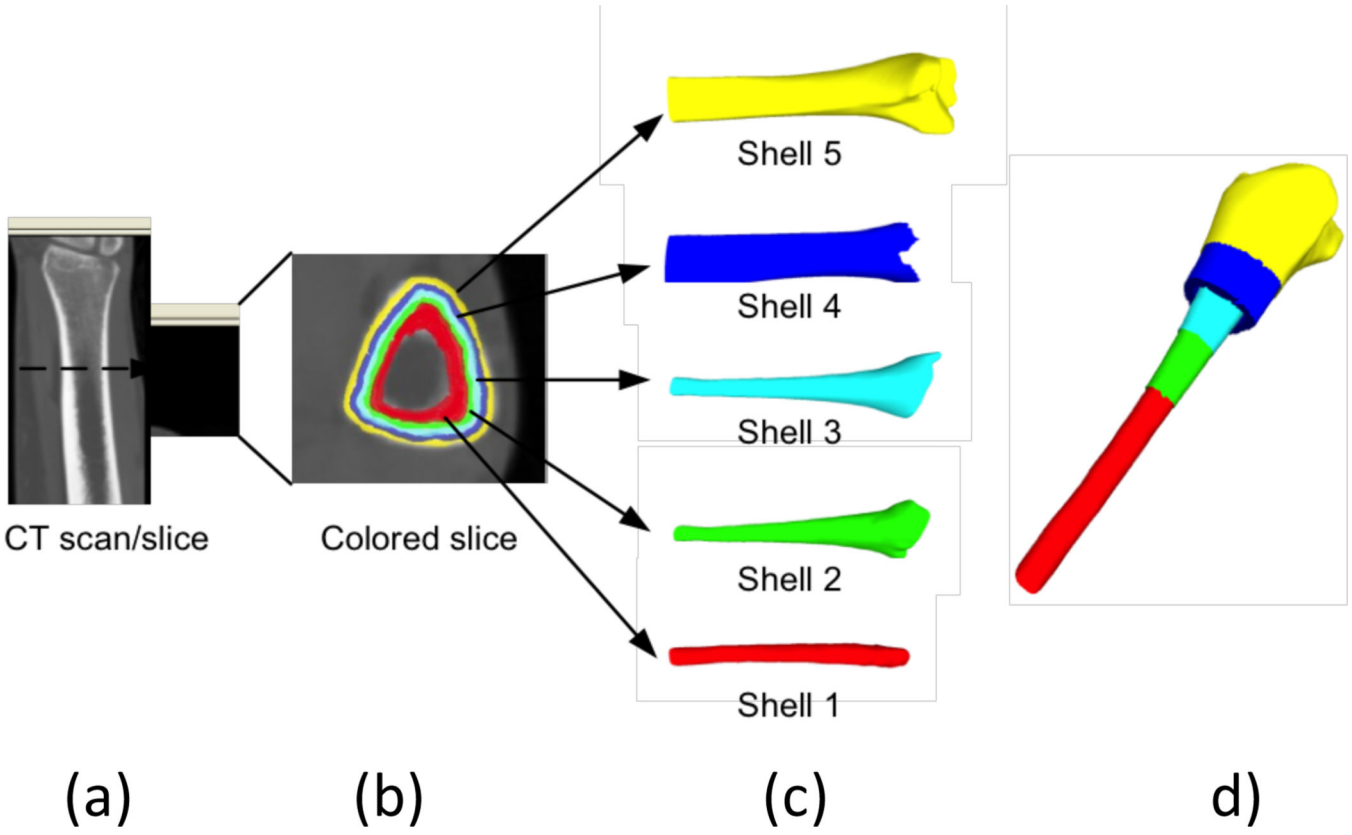

Figure 7.

Matryoshka model of the human tibia. (a) CT Scan and slice; (b) View of colored cross-sectional geometry; (c) Five shells generated from the medullary canal to outer bony surface; (d) Cut-away view of an assembled final model.

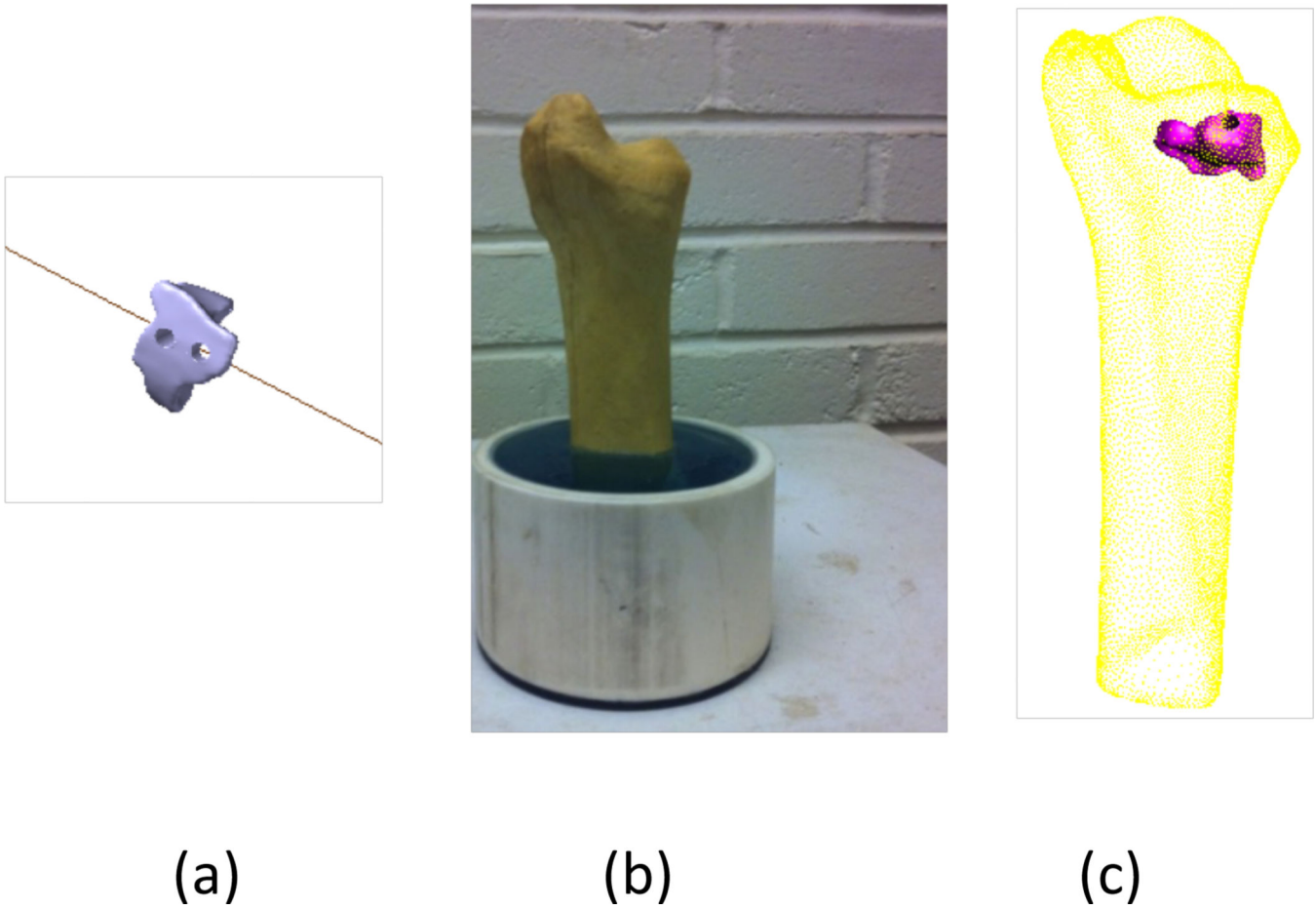

Figure 8.
Illustration of harvesting an implant from a desired location within the donor bone. (a) A CAD model of the implant; (b) A surrogate potted tibia bone; (c) The selected harvest location within the donor bone.

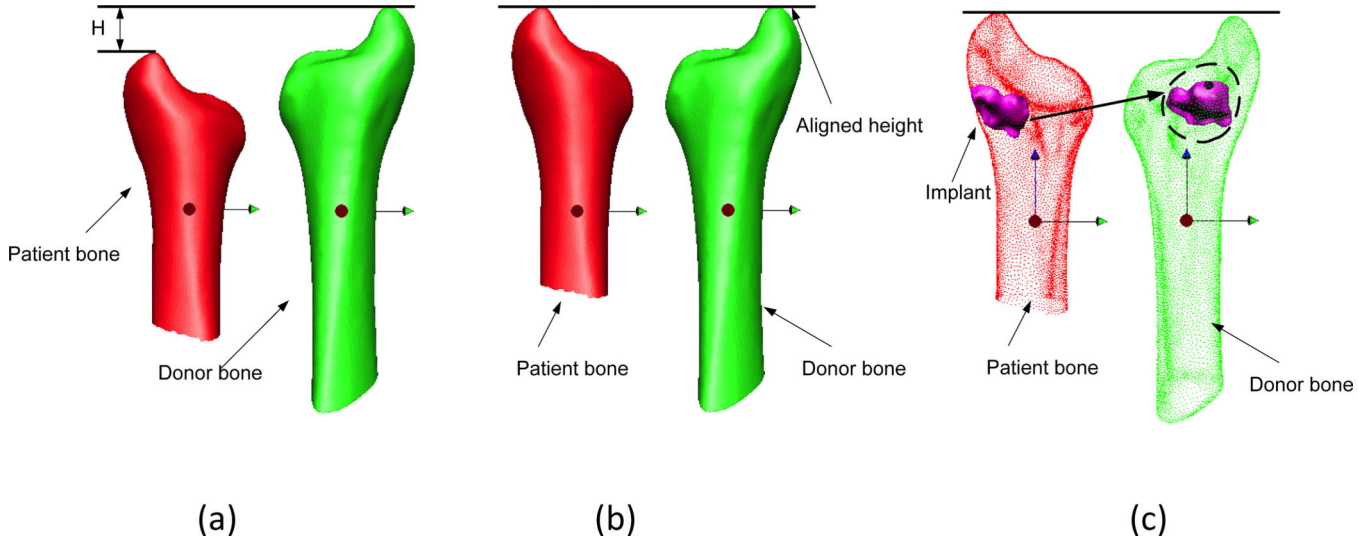

Figure 9.

An example of aligning the ends of the bones. (a) Before alignment; (b) After alignment; (c) Implant geometry from patient bone transferred to donor bone.

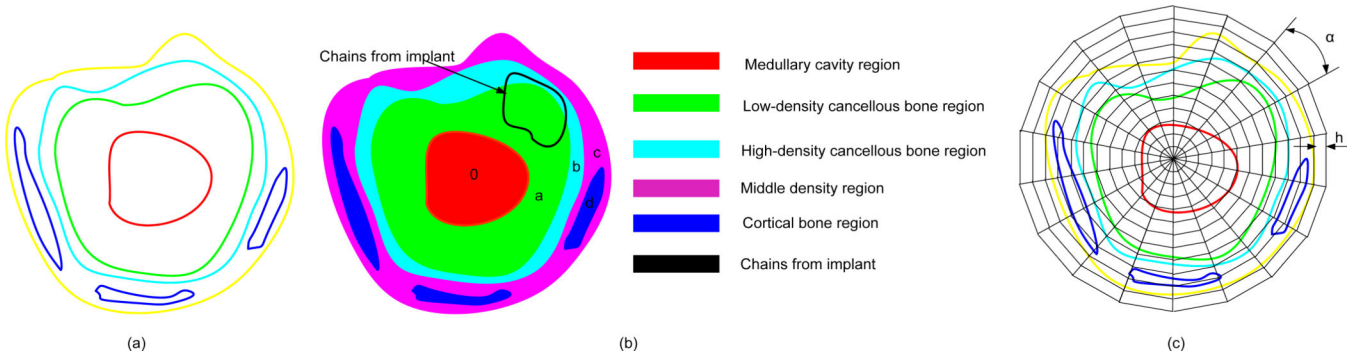

Figure 10.

(a) One cross-section from Matryoshka shell model; (b) Color mapping for different density regions; (c) Discretized density regions.

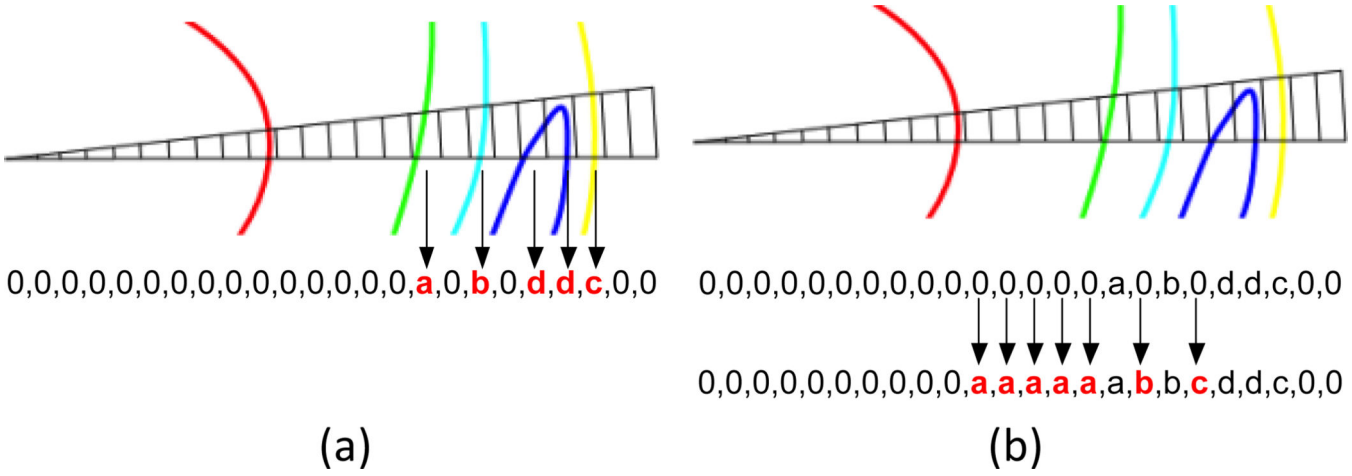

Figure 11.
Section chains intersecting the grid elements. (a) Shell boundary detection; (b) Element fill.

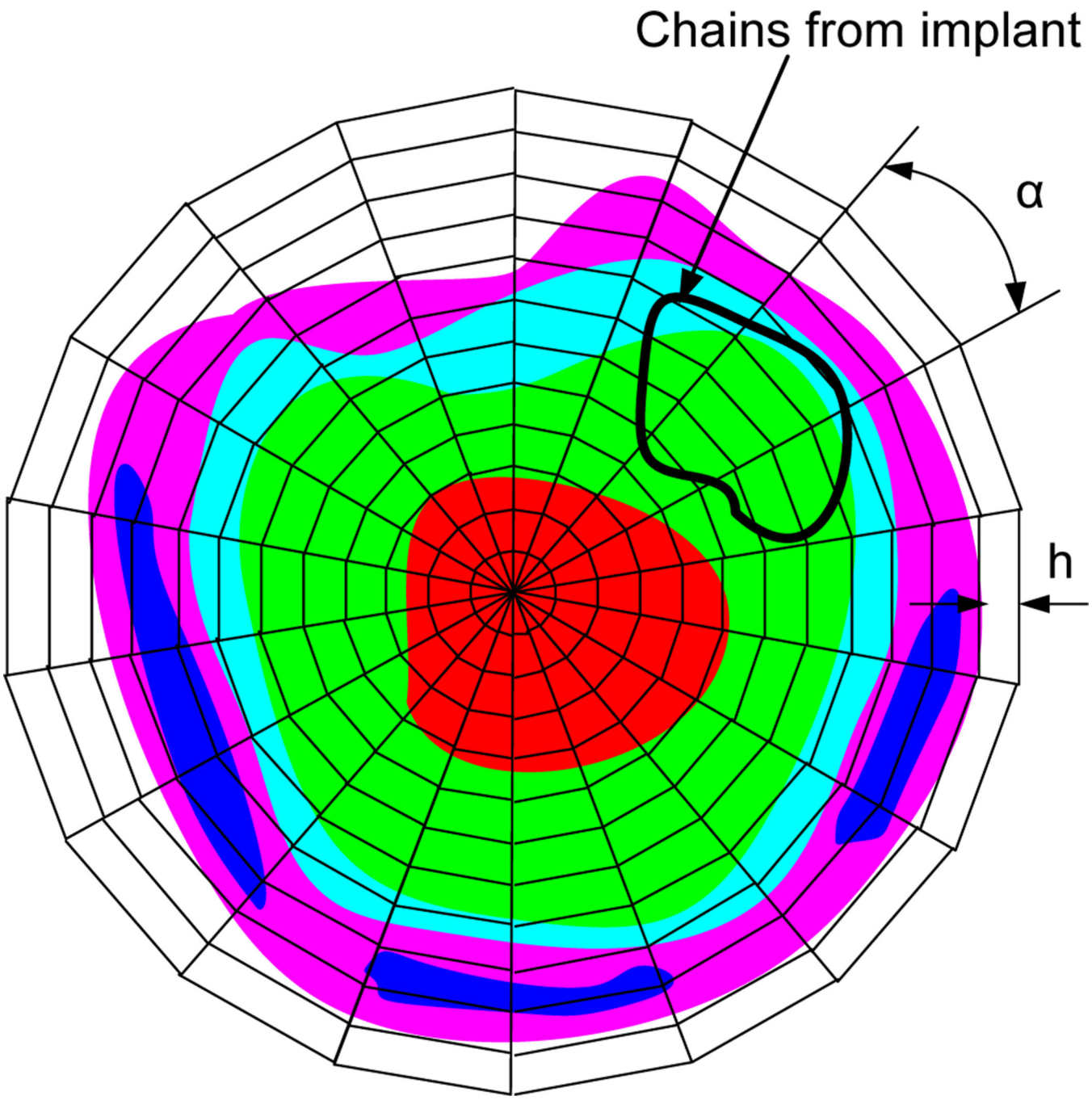

Figure 12.
Color mapping in grid structure.

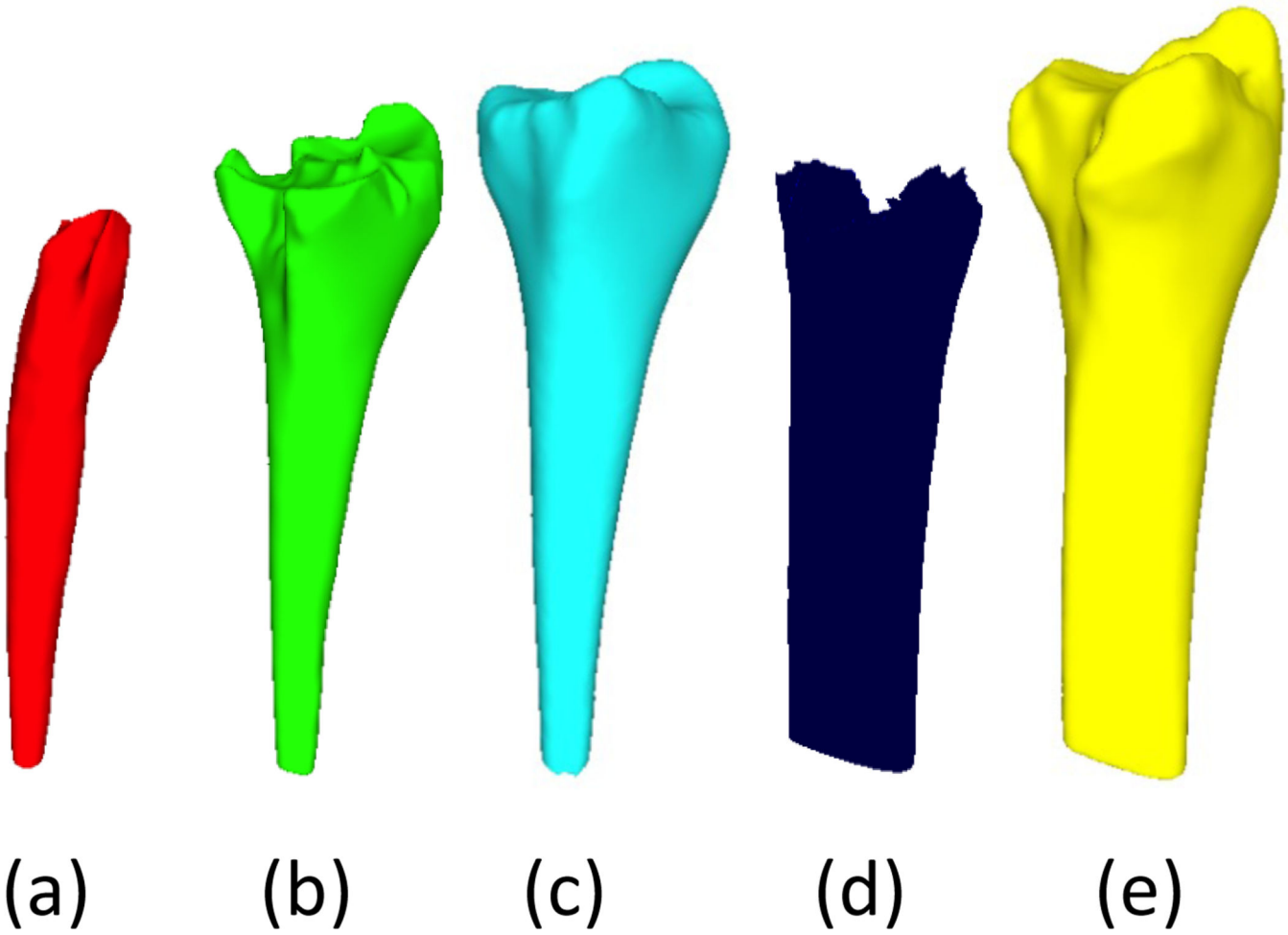

Figure 13.
A Matryoshka shell model of a human tibia. (a) Shell 1 (210HU); (b) Shell 2 (350HU); (c) Shell 3(HU500); (d) Shell 4(850HU); (5) Shell 5(1500HU).

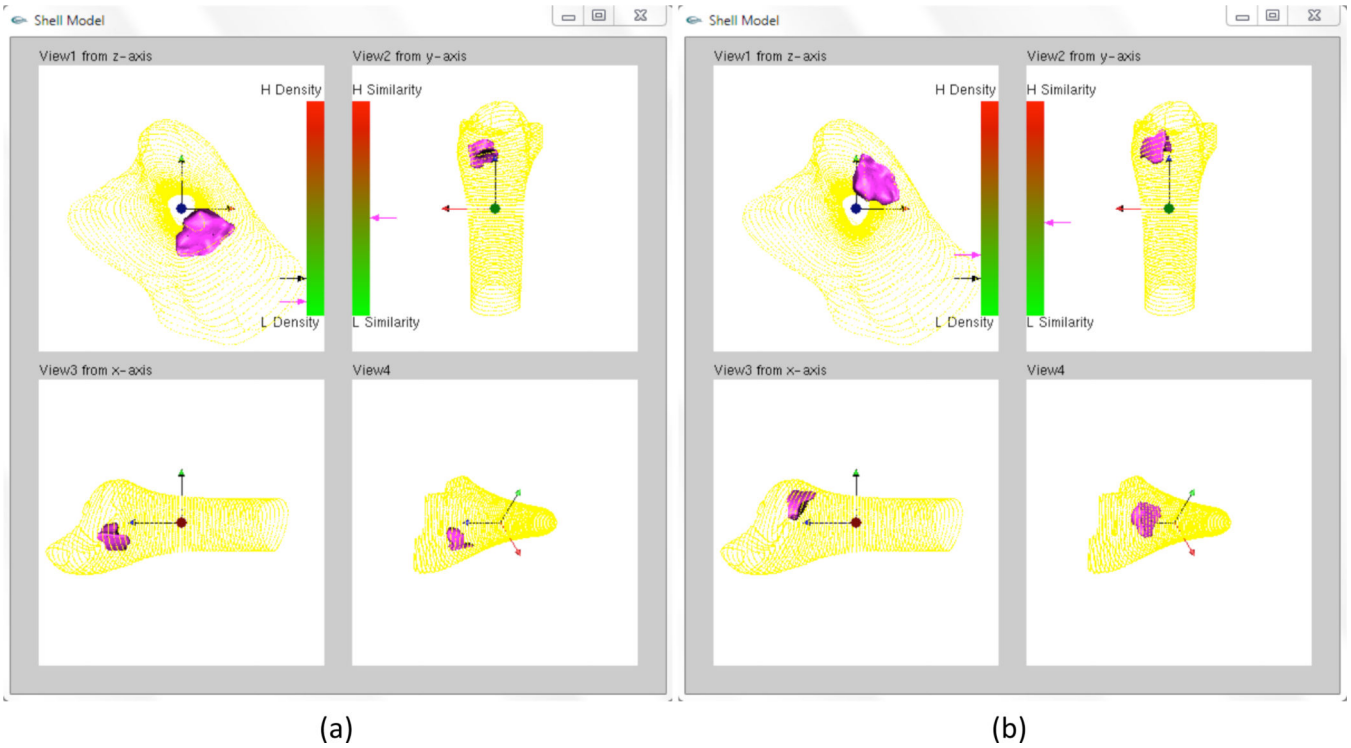

Figure 14.

Implementation results for two provisional implant harvest sites. (a) Initial location of the implant within the donor bone; (b) The location of the implant is updated by rotating about the *Z*-axis by 103.5°, translating along the *Z*-axis direction by −4.0 mm, and moving radially by 1.0 mm.

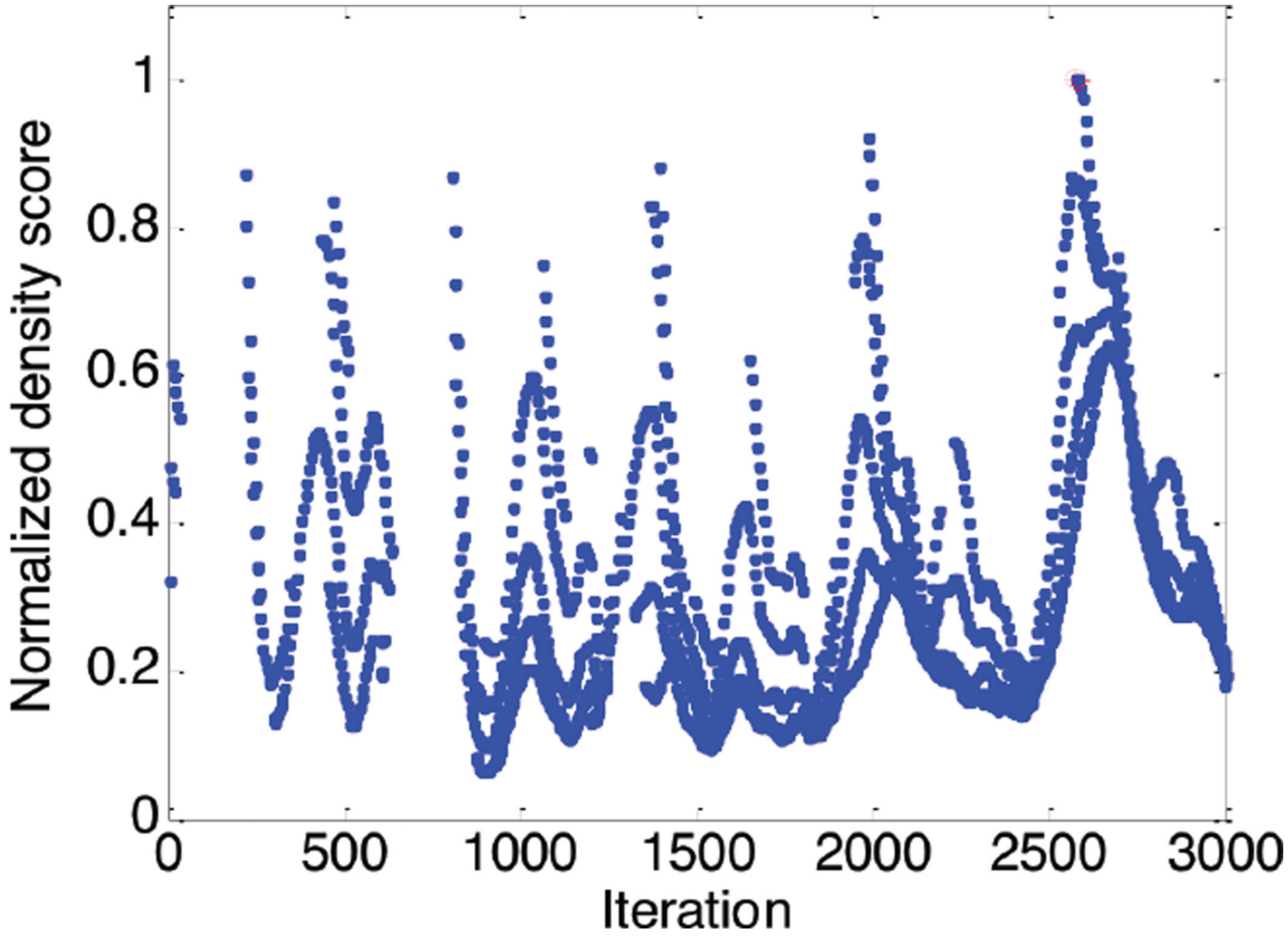

Figure 15.
Plot of normalized density score showing iterations

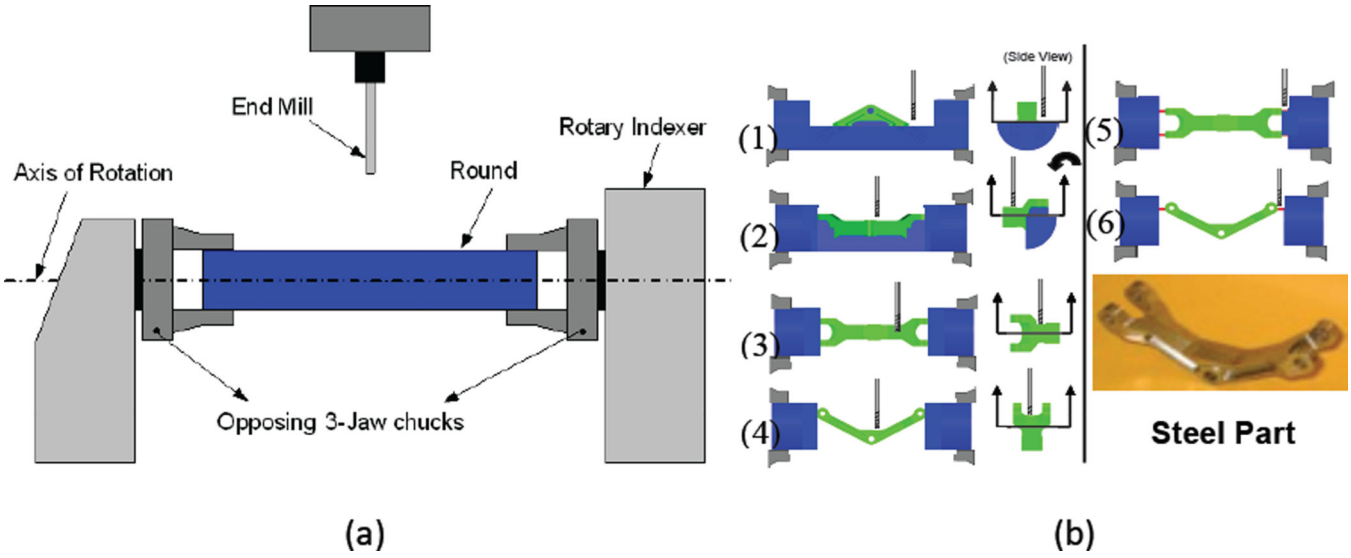

Figure 16.

CNC-RP Subtractive RP process (a) CNC-RP Fixture Setup; (b) Process sequence of steps (b.1–b.4) to expose component geometry and (b.5–b.6) to expose sacrificial supports.

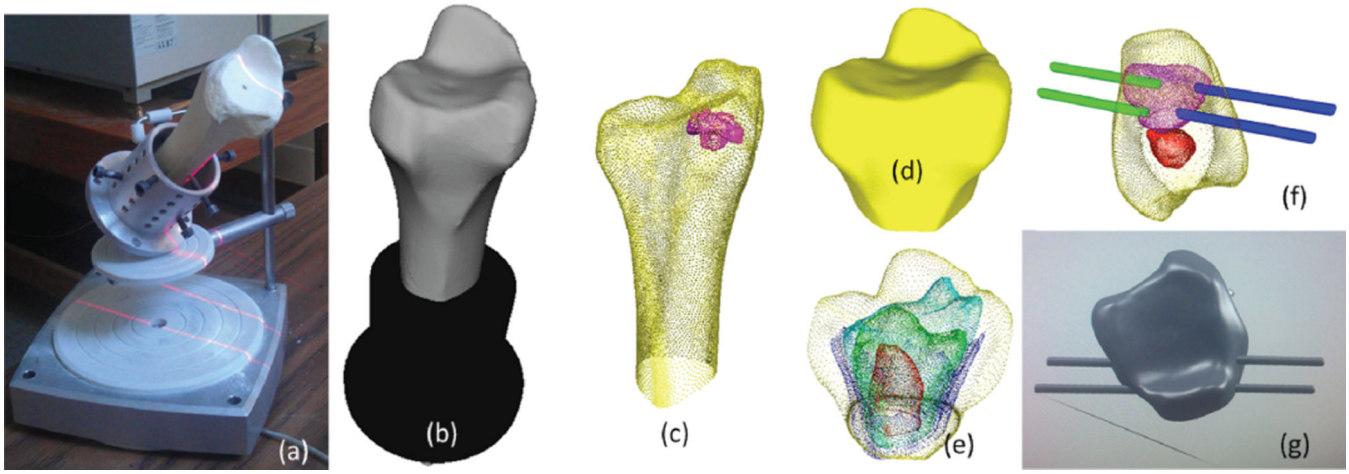

Figure 17.

Initial preparations for implant harvest. (a) Stock bone in the fixture pot; (b) CAD model of scanned bone; (c) Harvested implant located within the bone; (d) Bone cut section; (e) Matryoshka shells in bone cut section; (f) Sacrificial support generation; (g) Supports are placed in the CAD model.

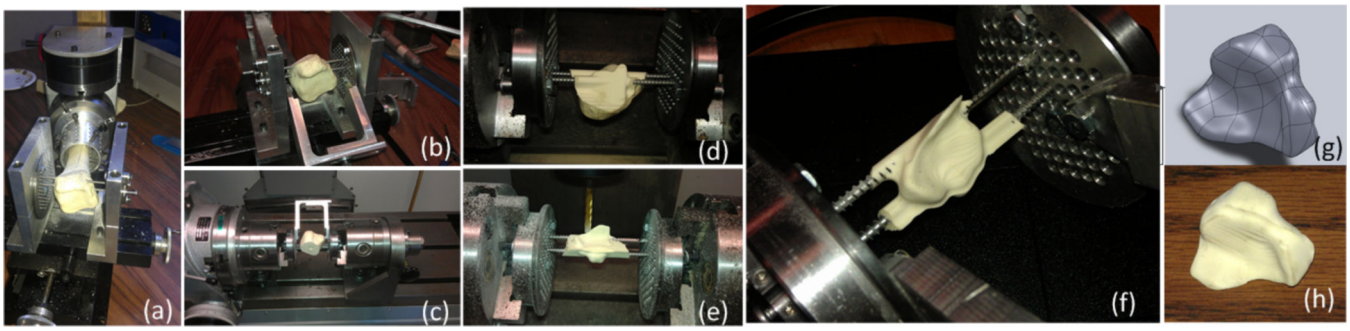

Figure 18.

Implant harvesting using CNC-RP. (a) 5-axis rotation device places the bone between the disks; (b) Cut section of the bone used for machining the implant; (c) Disks are placed in chucks for machining; (d) and (e) Machining from different angles; (f) Finished implant; (g) Original implant CAD model; (h) Machined implant with supports removed.